Int J Adv Manuf Technol (2012) 61:559–567
DOI 10.1007/s00170-011-3739-y

ORIGINAL ARTICLE

Effect of laser post-treatment on Al_2O_3-TiB_2-TiN composite coating with free hBN

Satyajit Chatterjee · J. Dutta Majumdar · S. M. Shariff · G. Padmanabham · A. Roy Choudhury

Received: 25 April 2011 / Accepted: 3 November 2011 / Published online: 7 December 2011

Abstract The development of nanostructured, hard, and wear-resistant composite coating of Al_2O_3, TiB_2, and TiN on low carbon steel (AISI 1025) substrate by combined self-propagating high-temperature synthesis (SHS) and laser surface alloying (LSA) has already been communicated in the author's previous publications. The coefficient of friction of the coating (with WC-Co as counterbody) is also found to have reduced substantially with the presence of free hexagonal boron nitride (hBN) in it. The occurrence of free hBN has been made possible by putting excess hBN in the precursor mixture which is supposed to undergo combined SHS and LSA. This has also been reported in one of the previous publications. This reduction in coefficient of friction is achieved at a cost of a marginal reduction in the microhardness as well as the specific wear rate as the free hBN in the coating matrix causes some softening. Laser post-treatment causes distinct enhancement in the microhardness and wear resistance of the coating while augmenting the favorable effect of free hBN on the coefficient of friction.

Keywords Laser alloying · SHS · Post-treatment · Nanostructured · Pin-on-disk · Coefficient of friction

1 Introduction

A considerable amount of research investigation is being carried out to develop low-friction protective layers on surfaces of engineering components subjected to relative motion. Certain phase components incorporated inside the coating may act as solid lubricants so that the common practice of application of expensive, hazardous, and messy lubricants can be avoided. Under severe tribological conditions, where the application of conventional lubricants may be undesirable, impractical, or ineffective due to presence of excessive temperature, load, speed, fluid contamination, vacuum environment, leakage, or any other unacceptable circumstance, a viable alternative could be the employment of a solid lubricant.

Presently, solid lubricants like diamond-like carbon and molybdenum disulfide (MoS_2) are widely applied in the industry. MoS_2, WS_2, and graphite are known to have lubricating properties owing to the ease of shearing of the bonds between the planes of atoms in the atomic structures of these materials [1]. Hexagonal boron nitride (hBN) has a lamellar crystalline structure which is similar to those of graphite and MoS_2. This structure of hBN can easily be sheared along the basal plane of hBN, thus qualifying its role as a solid lubricant additive. There are several research investigations that report the role of hBN in reducing friction in various tribological applications [2–4].

S. Chatterjee
Department of Mechanical Engineering,
Indian Institute of Technology,
Indore, MP, India
e-mail: satyajit@iiti.ac.in

J. D. Majumdar
Department of Metallurgical and Materials Engineering,
Indian Institute of Technology,
Kharagpur, WB, India

S. M. Shariff · G. Padmanabham
International Advanced Research Center for Powder Metallurgy and New Materials (ARCI),
Hyderabad, India

A. R. Choudhury (✉)
Department of Mechanical Engineering,
Indian Institute of Technology,
Kharagpur, WB, India
e-mail: archie@mech.iitkgp.ernet.in

Although there are many other solid lubricants present with excellent tribological properties, their applications as additives in coatings, their adherence/tendency to bond with other phases in the coating matrix and substrate and inadequate workability at higher temperatures have posed obstacles to their adoption as solid lubricants. A single solid lubricant may not provide adequate lubrication over a wide range of temperature and operating conditions and an approach towards the development of a coating with synergetic self-lubricating action (along with high wear resistance) can become very useful [5].

Laser surface alloying (LSA), as a surface engineering technique, involves melting of a pre-/co-deposited layer of alloying element(s) along with a part of the underlying substrate, leading to the formation of an alloyed zone confined to a very low depth from the top surface within a very short interaction time [6]. The primary advantage of LSA over conventional coating techniques is that novel microstructures can be produced due to inherently rapid solidification and high concentration of key elements at or near the surface. In addition, the coatings are metallurgically bonded to the substrate and their microstructures can be graded during processing to reduce thermal stress gradients occurring due to the thermal expansion mismatch between the coating and the substrate [7].

Self-propagating high-temperature synthesis (SHS) is a technique that leads to the in situ formation of compounds from reactant substances through exothermic reaction [8–13]. SHS provides an energy-efficient approach to the synthesis of materials including solid solutions, composite materials, and metastable phases. The specialty of this process is the conversion of chemical energy to thermal energy and its ability to self-sustain the reaction, once triggered. The products are generally of high purity due to volatilization of impurities [14, 15]. Laser-assisted or laser-triggered SHS has also been investigated by some researchers [16–18].

The development of nanostructured ceramic matrix composite coating of Al_2O_3-TiB_2-TiN having sufficiently high hardness with fine, homogeneous microstructure, through combined SHS and LSA route has already been reported by Chatterjee et. al. [19–22]. A precursor mixture of aluminum (Al), titanium-di-oxide (TiO_2), and hBN powders is preplaced on low carbon steel substrate and is subsequently scanned by laser to produce the alloyed coating by combined SHS and LSA. The stoichiometric proportions of the reactants constituting the precursor powder are taken as per Eq. 1 [19–23] with weight proportions mentioned below the reactants and their products.

$$\begin{array}{l} 4Al + 3TiO_2 + 2BN = 2Al_2O_3 + TiB_2 + 2TiN + 2303K \\ 10 \quad 22.39 \quad 4.638 \quad 19.05 \quad 6.49 \quad 11.56 - (\text{stoichiometric proportion}) \end{array} \tag{1}$$

The authors have also studied the scope of application of hBN as a solid lubricant in the present type of coating. Additional amount of hBN (in excess of the amount required as per Eq. 1) was incorporated in precursor mixture to obtain free hBN in final matrix, in addition to the hard phases Al_2O_3-TiB_2-TiN [20]. This excess hBN was found to act as a solid lubricant during relative motion of the coating with standard hard and wear-resistant engineering materials. It was observed that although the coating with increasing amount of hBN in the precursor mixture shows significant reduction of coefficient of friction in a sliding wear condition, the microhardness as well as specific wear rate suffers marginal reduction.

Laser post-treatment is a very effective technique for improving surface quality. It can be used to densify the topmost layer of the coating and thus increase its top

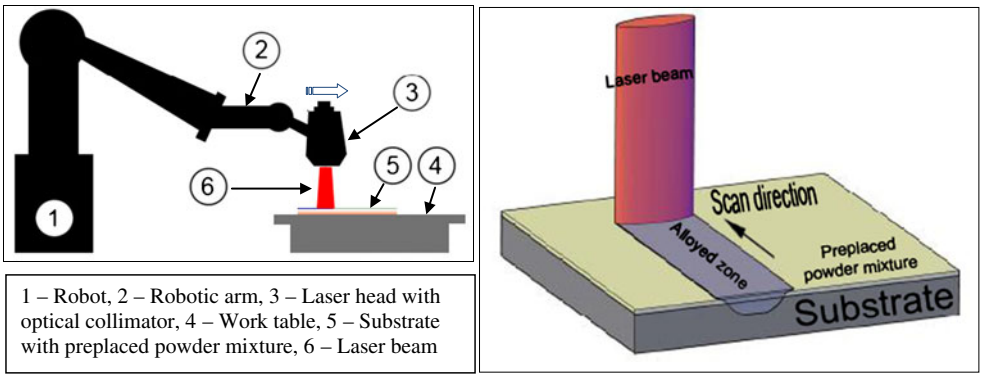

1 – Robot, 2 – Robotic arm, 3 – Laser head with optical collimator, 4 – Work table, 5 – Substrate with preplaced powder mixture, 6 – Laser beam

(a) (b)

Fig. 1 Schematic diagram of **a** test setup and **b** laser surface alloying of preplaced powder mixture

Table 1 Components of the laser surface alloying test set up

Sl No.	Name of the component	Utility
1	Robot	Helps in maneuvering the laser head
2	Robotic arm	Helps the laser head in reaching the laser beam in the desired position
3	Laser head with optical collimator	Helps in getting the desired characteristics of the laser beam
4	Work table	Provides perfectly flat and horizontal workspace for samples
5	Substrate with preplaced powder mixture	Test piece
6	Laser beam	Performs laser surface alloying

hardness and seal it against penetration by corrosive agents. High-power laser beam may be used to melt the top layer of the surface, followed by rapid cooling leading to formation of refined microstructure with improved properties. Laser post-treatment leads to refinement and homogenization of microstructure and hence, may be applied to tailor the surface-dependent properties of material. Besides this, laser post-treatment alters microstructures without changing the composition and provides a smooth, dense top layer [24]. The authors have already investigated the tribological behavior of Al_2O_3-TiB_2-TiN coating developed by laser surface alloying. The effect of laser post-treatment on the tribological behavior of the coating has also been studied [21]. Incorporation of additional amount of hBN in the coating was observed to improve the frictional property of the matrix [20]. In the present study, an attempt has been made to determine the effect of laser post-treatment on the mechanical properties of the coating produced with incorporation of additional amount of hBN in precursor. The motivation of this present work would be to investigate the possibility to overcome the loss of hardness and wear resistance due to the presence of free hBN in final matrix to obtain a solid lubricious coating with sufficiently high hardness and wear resistance.

2 Experimental details

Steel samples [AISI 1025, size: 100×50×8 mm^3], surface ground (R_a, 0.2 μm), are used as substrates for LSA. The precursor powder mixture (for initial SHS reaction) consists of titanium-di-oxide (Rutile, particle size, 1.0–2.0 μm; purity, 99.5%; manufacturer Alfa Aesar), hexa-boron nitride (−325 mesh; purity, 99.5%; manufacturer, Alfa Aesar), and aluminum (particle size, ~10 μm; purity, 99.7%; manufacturer, Loba Chemie) in the stoichiometric proportion as per chemical reaction depicted in Eq. 1. Measured quantities of these powders along with calibrated amount of a poly-urethane based adhesive (Dendrite, PU-201) are mixed in acetone (supplied by Merck; water content, ≤0.3%) by alternate cycles of mechanical stirring (by a magnetic stirrer, Remi Equipments, 1 MLH) and ultrasonic vibration (ultrasonic vibrator, Systronics; model, 1201). After mixing, the powder-acetone blend is applied manually on the AISI 1025 steel substrate surfaces with a smooth paintbrush up to a thickness of 100 μm. Prior to application of precursor powder mixture, sample surfaces are thoroughly cleaned with acetone. After allowing the coating to dry thoroughly, the samples are baked in furnace at a temperature of 100°C for a period of 5 min in argon atmosphere for setting the adhesive and for the complete removal of moisture and volatile materials. The samples are subsequently furnace cooled to room temperature.

LSA is carried out with a continuous wave (CW), 1,500 μm, fiber-coupled diode laser (model, LDF 6000; Laserline, Germany) having a power range of 200–6,000 W (wavelength, 915–980 nm), integrated with an eight-axis robotic workstation (Reis Robotics, Germany). A multi-mode (with uniform intensity distribution in front axis and Gaussian intensity distribution in slow axis) rectangular laser beam of spot size 17×2 mm^2 with homogenous

Table 2 Powder compositions and the laser parameters for different Samples

Samples		Samples without laser post-treatment				Samples with laser post-treatment			
		M11	M12	M13	M14	G11	G12	G13	G14
LSA parameters		4.5 kW, 20 mm/s							
Composition	Al (g)	1							
	TiO_2 (g)	2.24							
	hBN (g)	0.46	0.92	1.38	1.84	0.46	0.92	1.38	1.84
Laser post-treatment parameters		NA				2 kW, 60 mm/s			

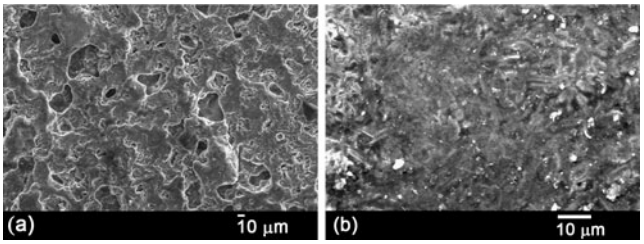

Fig. 2 Scanning electron micrograph of the top surface of two representative coatings; **a** without laser post-treatment and **b** with laser post-treatment

intensity obtained with a special optical setup (comprising integrating, homogenizing, and focusing optics) has been used for scanning the precursor surface. An argon shroud jet with 1 bar pressure, covering entire laser beam area has been provided during processing to avoid atmospheric contamination. Figure 1a, b schematically represents the CW diode laser setup for the experiment and laser surface alloying of preplaced powder mixture. Different components of the setup along with their usage are enlisted in Table 1.

Table 2 elucidates the proportions of the constituents of the precursor powder mixture, along with processing parameters (laser power and scan speed) employed for different samples. Coatings produced by combining SHS and LSA are named as M1. The composition of the preplaced powder mixture in case of sample M11 of Table 2 was prepared according to the chemical reaction shown in Eq. 1. The amount of hBN has been increased in the precursor powder mixtures in three equal weight increments from samples M12 to M14, respectively. The top surface of the coatings developed by combined SHS and LSA (M1 coatings) are subsequently laser post-treated with a different set of laser parameters (laser power and scan speed). These samples are referred to as G1 coatings. Laser post-treatment parameters are also summarized in Table 2.

Specimens with laser-treated layers were characterized with respect to microstructural, mechanical, and tribological properties. Microstructural characterizations were carried out on a Zeiss EVO-60 scanning electron microscope (SEM) and a Zeiss Supra-40 field emission scanning electron microscope. The chemical compositions of the coatings were qualitatively evaluated in elemental mapping mode with the help of energy dispersive spectroscopy coupled with SEM. X-ray diffraction analysis of the coated surfaces were obtained with a PHILIPS Rayons-X ray diffractometer with Co-K_α radiation. Bright field imaging and selected area diffraction patterns combined with dark field imaging were studied on a JEOL JEM 2100 high-resolution transmission electron microscope (HRTEM) for detection and identification of nanophases.

The microhardness of the coating cross-section was measured with a microhardness testing machine (Leco-LM700) using 50 g load (dwell time 15 s). The Vickers Diamond Pyramid indenter used for this measurement has a shape of a squared pyramid with an angle of 136° between faces. In order to assess tribological improvement of the coatings due to laser post-treatment, sliding wear tests were carried out with a tribometer (*DUCOM - TR-201-M3*) and the results were compared with those obtained from sliding wear tests applied on coatings without laser post-treatment. The testing involves dry sliding of a cemented WC-Co ball (φ5, make, SALEM; WC, 93.5–94.5%; Co, 5.5–6.5%) against laser-treated surface of the specimen at a specific sliding speed and normal load stated in the relevant section. The wear coefficients were calculated by measuring wear track depths using a stylus profilometer (Taylor-Hobson Surtronic 3+).

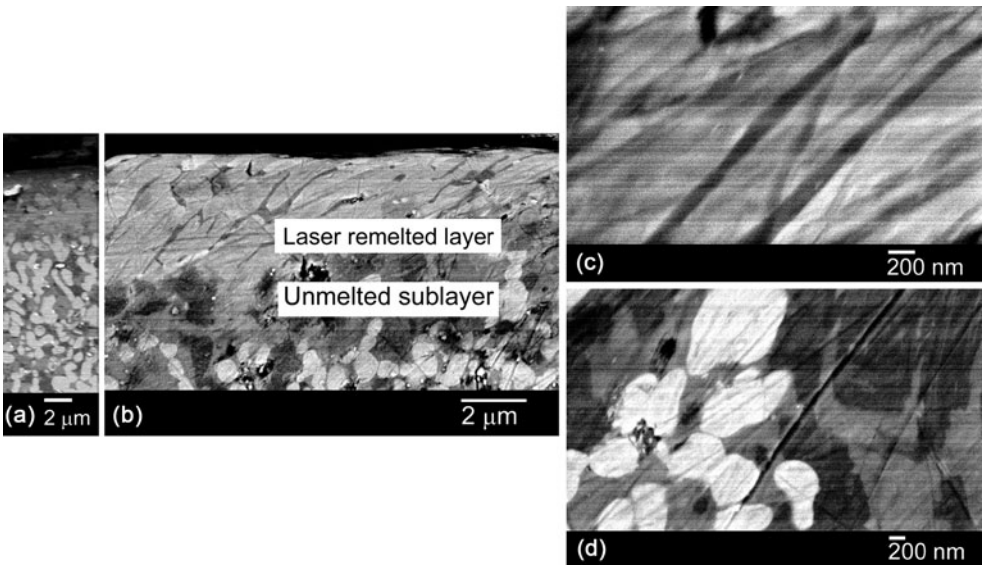

Fig. 3 Scanning electron micrograph of the cross-section of the coating **a** without laser post-treatment and **b** with laser post-treatment followed by high magnification view of **c** top melted layer and **d** bottom layer

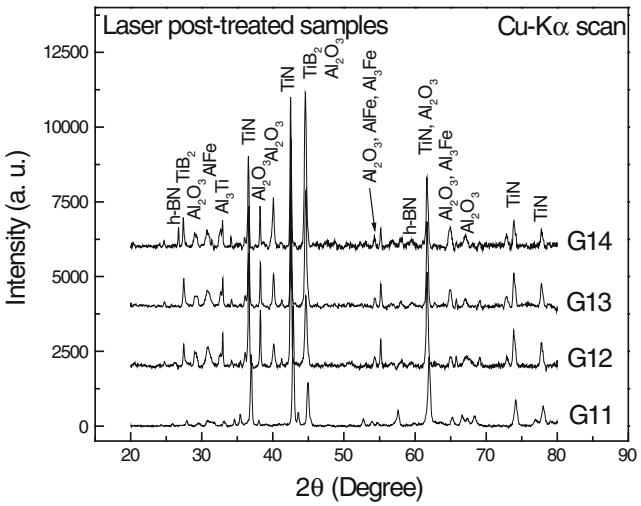

Fig. 4 X-ray diffraction profiles of the coated samples (G11, G12, G13, and G14) formed with combined SHS and LSA followed by laser post-treatment. The samples are prepared with varying amounts of hBN in precursor mixture. Amount of hBN: **a** G11→stoichiometric amount as per Eq. 1 **b** G12→twice the stoichiometric amount as per Eq. 1, **c** G13→thrice the stoichiometric amount as per Eq. 1, **d** G14→four times the stoichiometric amount as per Eq. 1

3 Results and discussion

The coating consists of three phases—Al_2O_3, TiB_2, and TiN where TiB_2 and TiN act as reinforcing phases in a matrix of Al_2O_3. The constituent phases of the coating are actually the reaction products generated from a laser triggered SHS reaction between Al, TiO_2, and hBN preplaced as a precursor powder mixture on the steel substrate. The products of the reaction subsequently form the coating through LSA process. In one of the authors' previous publications, a study has been carried out on the effect of addition of excess hBN (in the precursor powder) on the properties of the final laser surface alloyed coating [20]. The amount of hBN in excess of the stoichiometric amount, remains in the coating matrix as free hBN and acts as solid lubricant. In the present study, the coating with excess hBN in the precursor mixture is made to undergo laser post-treatment. This causes reduction in the detrimental effects of free hBN on the hardness and wear resistance of the coating while augmenting the favorable effect of free hBN on the friction coefficient.

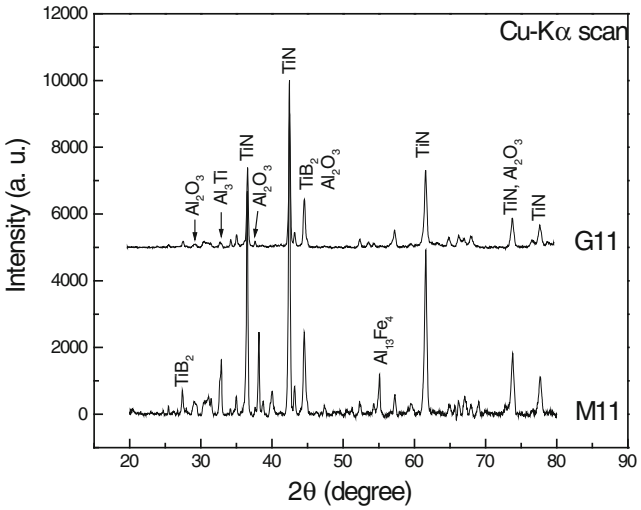

Fig. 5 X-ray diffraction patterns of the coated samples (G11 and M11) produced with and without laser post-treatment. Both the samples have stoichiometric amount of hBN (as per Eq. 1) in the precursor powder mixture

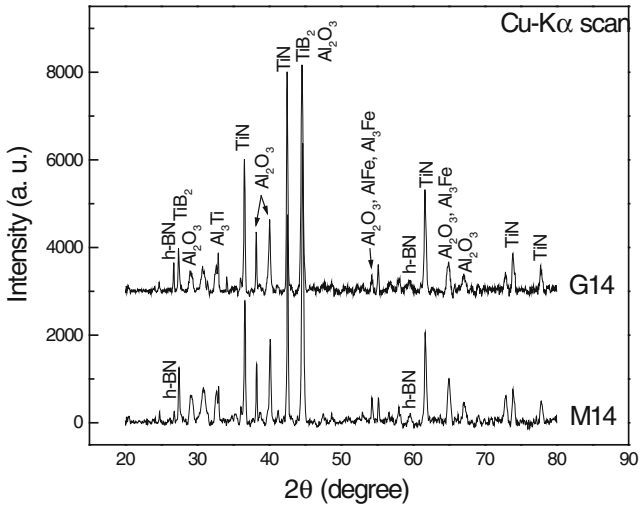

Fig. 6 X-ray diffraction patterns of the coated samples (G14 and M14) produced with and without laser post-treatment. Both the samples have four times than the stoichiometric amount of hBN (as per Eq. 1) in the precursor powder mixture

Figure 2a, b shows the SEM micrographs (secondary electron mode) of the top surface of the coatings without and with laser post-treatment. It is clearly visible that the

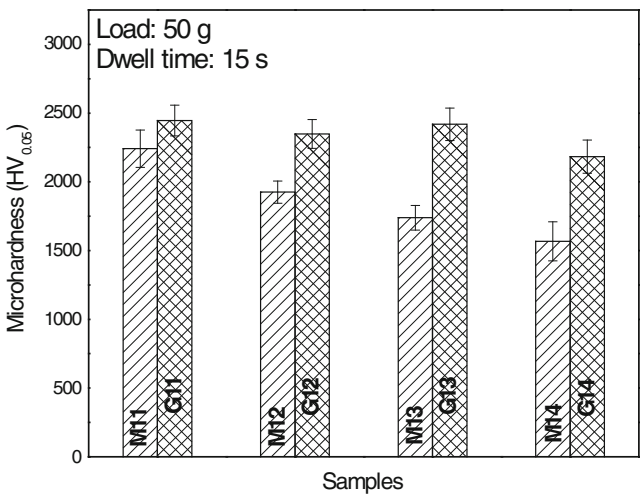

Fig. 7 Average microhardness values obtained at the top 25 μm of the coating cross-section of all the coated samples produced with and without laser post-treatment

Table 3 Operating conditions used on ball-on-disk experiment for friction and wear measurement

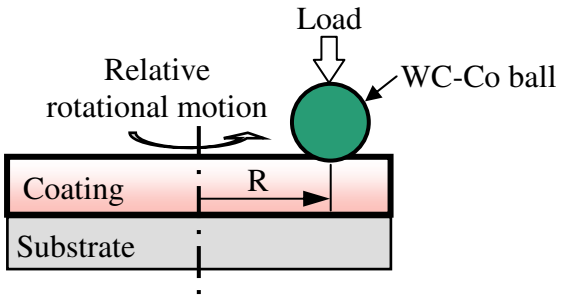

Operating conditions	
Cemented tungsten carbide (WC-Co) ball diameter	5 mm
Track diameter (2R)	5 mm
Load	1 kgf
Sliding distance	~ 113 m

coating produced with laser post-treatment has relatively smoother top surface (Fig. 2b) as compared to that of the coating without laser post-treatment (Fig. 2a). This is affirmed by the comparison of surface roughness parameters (maximum and average) for the two types of surfaces with the help of a surface profilometer. In the case of the

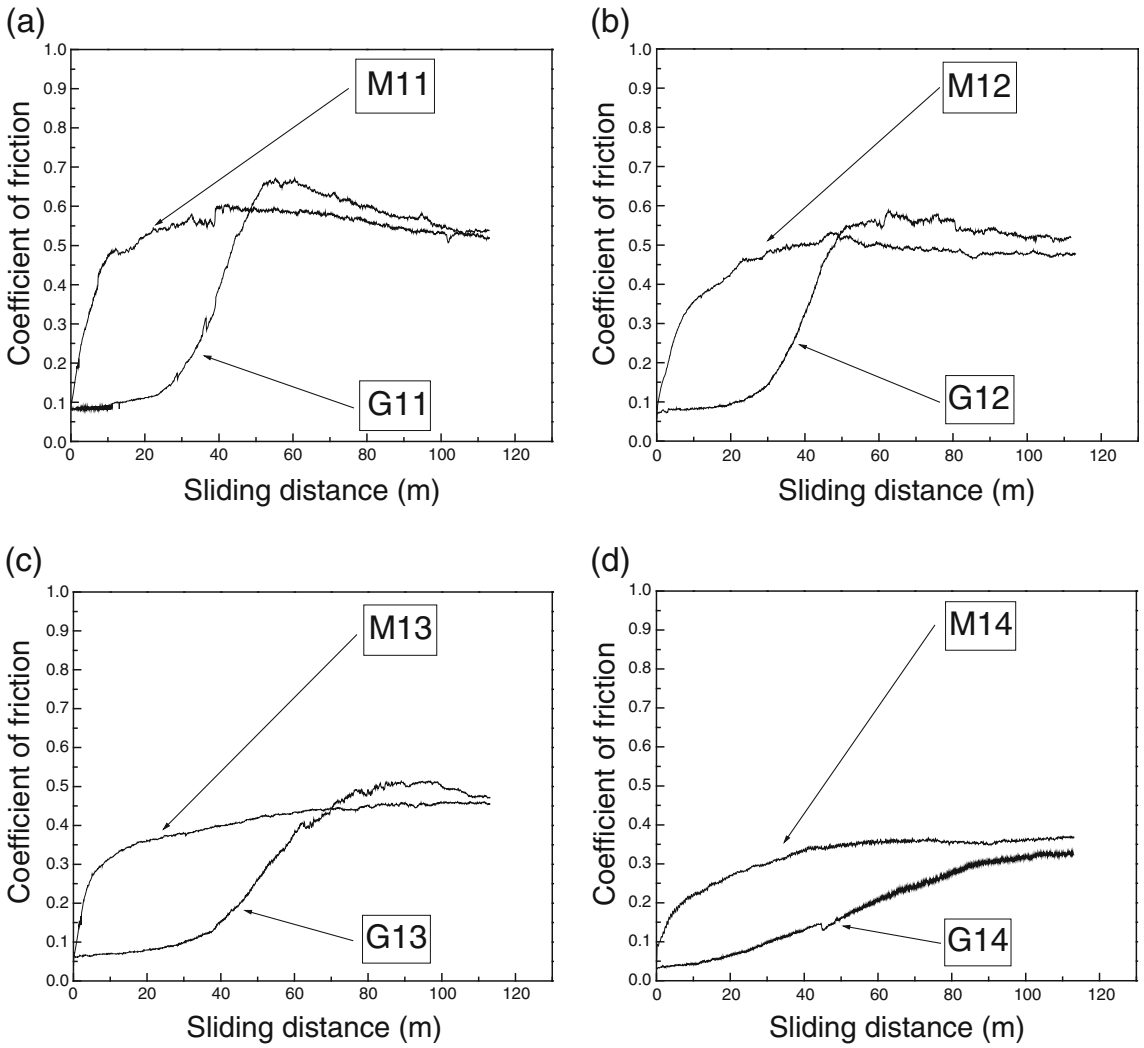

Fig. 8 Comparison of coefficient of frictional of samples (G11 and M11, G12 and M12, G13 and M13, G14 and M14) to find out the effect of laser post-treatment on samples with free hBN in the coating

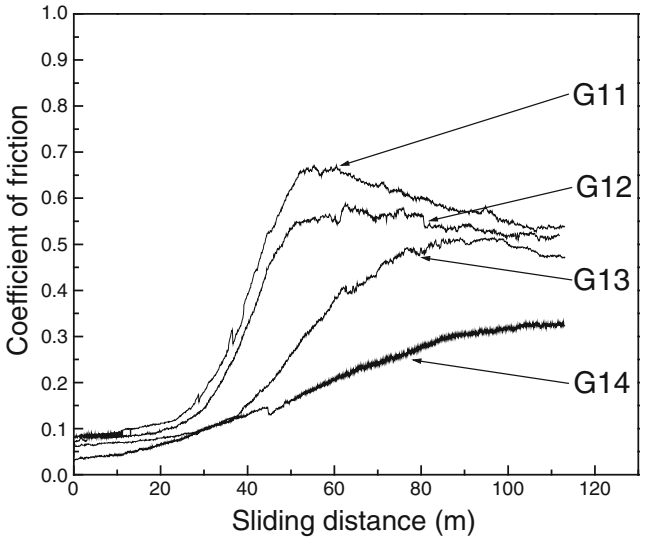

Fig. 9 Comparison of coefficient of friction of laser post-treated samples (G11, G12, G13, and G14) to find out the effect of free hBN in the coating on samples with laser post-treatment

sample without laser post-treatment, there is the presence of small surface porosity at the top surface (as can be seen from Fig. 2a) typically up to a size range of 80–90 μm. Scanning electron micrographs (back-scattered mode) of the cross-section of coating without and with laser post-treatment are shown in Fig. 3a–d. Figure 3a shows the cross-section of coating without laser post-treatment. A considerable amount of change is visible at the coating cross-section (Fig. 3b–d) after laser post-treatment. From Fig. 3b, c it is very clearly visible that the top portion of the coating has a distinct columnar structure, growing along the direction of heat flow, significantly different from the lower part (Fig. 3d) of the coating. The lower part of the coating is predominantly a uniform dispersion of small [~500 nm] globular and acicular titanium-rich phases in an aluminum-rich matrix.

In LSA, the products of the SHS reaction get melted by the scanning laser. The constituent phases of the coating have widely different solidification temperatures (e.g., TiB_2, 3,225°C; TiN, 2,950°C; Al_2O_3, ~1,900°C). When the melt pool solidifies, first, the phases with higher melting points tend to get solidified and acquire globular or acicular shape due to very high rate of cooling. This causes the melt pool to get segregated to many smaller ones containing mainly molten Al_2O_3 and TiAl and already solidified TiB_2 and TiN phases. As the solid/liquid interface advances with decrease in temperature, the grains continue to grow and hence cover up the rest of the areas. Now, at certain time, the grains growing at some of the fusion boundaries get blocked by the grains already grown at another cooler part of the melt pool. This gives a randomly oriented grain structure. In case of the coating produced by combined SHS and LSA, SHS reaction sets in with the strike of the laser on the surface of the preplaced powder. SHS results in very fine-grained reaction products which melt very easily by the heat inputs from laser as well as from the ongoing highly exothermic SHS reaction. Due to lower particle size, the products of SHS would have a higher surface-to-volume ratio leading to higher absorption of heat which would facilitate melting in case of SHS+LSA [21, 25].

In laser post-treatment process, irradiation by a high power scanning laser leads to melting of a thin top layer of the coating, followed by rapid solidification. Frequently, in the process, nanoparticles in the coating get easily diffused in the melt pool on account of their high diffusion coefficient. These nanoparticles can act as nucleation sites during rapid solidification resulting in non-direction growth of crystals. Hence, fine, homogeneously distributed equi-axed grains could be obtained in the coating depending upon the processing conditions involved.

X-ray diffraction patterns of the coated samples formed with combined SHS and LSA followed by laser post-treatment are shown in Fig. 4. Apart from the presence of Al_2O_3, TiB_2, and TiN, the presence of hBN is also revealed in samples with additional amounts of hBN in the precursor powder mixture. This is corroborated by the HRTEM and XPS results presented in the authors' previous publication [20]. Figure 4 also evidences the formation of titanium aluminide and iron aluminide (Al_3Ti, AlTi, $AlFe_3$, etc.) in the coating. X-ray diffraction patterns of the samples with and without laser post-treatment are also compared in Figs. 5 and 6. Figure 5 represents the comparison between the diffraction data of samples G11 and M11 whereas Fig. 6 depicts the same between G14 and M14. In both the figures, change in the intensity of several phases before and after laser post-treatment is noticeable.

Microhardness values are measured on a number of cross-sections for each coating. Figure 7 shows the average microhardness values obtained at the top layer (of 25 μm thickness) of the cross-sections of the coatings. It is observed that there is a distinct increase in the value of the average microhardness of the top layer after laser post-

Table 4 Values of specific wear rate of the samples

Samples	M11	G11	M12	G12	M13	G13	M14	G14
Specific wear rate ($mm^3/N-m$; for sliding distance=~113 m)	9.80E-05	9.11E-05	1.11E-04	1.03E-04	1.22E-04	1.13E-04	1.37E-04	1.18E-04

Table 5 Percentage composition of samples obtained through RIR method

Name of the phases	Age in M14 sample (%)	Age in G14 sample (%)
TiN	10	8
Al_2O_3	55	44
TiB_2	11	22
hBN	3	15

treatment. This increase in hardness is possibly due to the refinement and compaction of the microstructure, together with the mechanism of strengthening of the microstructure, specifically Orowan strengthening effect [21, 26, 27]. Coatings with variable amounts of hBN were laser post-treated and the effect of this treatment on the friction and wear behavior of the coating was evaluated using a ball-on-disk tribometer against WC-Co ball at room temperature (26°C) with a relative humidity of 60±2%. The operating conditions for the tests are listed in Table 3.

Figure 8 depicts the effect of laser post-treatment on the coefficient of friction (COF) of coatings with varying amounts of hBN in the precursor powder mixture. The variation of COF against sliding distance for laser alloyed samples without laser post-treatment (i.e., samples with codes prefixed with M1 and made by SHS+LSA only) reconfirm the effect of increasing amounts of free hBN in the precursor powder (for coatings) on the tribological performance of the samples. There is monotonic decrease in the value of the coefficient of friction with the rise in the content of free hBN in the precursor mixture. However, plots of samples having same amounts of hBN in the precursor powder mixture (with and without laser post-treatment), viz., M11 and G11, M12, G12, etc., depict the effect of laser post-treatment on the coefficient of friction (Fig. 8). Figure 9 shows the combined effect of hBN and laser post-treatment on the COF of the coatings in sliding contact with WC-Co counterbody. Laser post-treatment considerably reduces the coefficient of friction in the initial part of the sliding friction as apparent from Fig. 9. Thereafter, the frictional behavior is governed by the hBN content in the coating matrix.

It may be observed (Table 4) that the wear rate tends to increase with the amounts of free hBN added in the precursor for the M1 coatings as well as for the G1 coatings. This is the negative effect of free hBN on the wear resistance of the coating. However, if the wear rates of the M1 and G1 samples are compared for the same LSA parameters, it can be noted that significant reduction in wear rate have taken place after laser post-treatment. This indicates that laser post-treatment causes improvement in the wear resistance of the coatings with free hBN. The increased wear resistance with laser post-treatment is attributed to increased hardness of the surface after laser post-treatment due to the refinement in microstructure. Hence, it may be concluded that laser post-treatment reduces the softening effect of free hBN on the wear resistance while augmenting the favorable effect of free hBN on the coefficient of friction.

The percentage composition of the phases is calculated at the surface of the coatings by relative intensity ratio (RIR) method. RIR is one of the simple and quickest ways to quantify X-ray diffraction data [28]. This diffraction data is available for the top surface of the coating. The amount of phases is evaluated by the X'Pert HighScore Plus® analysis package. The representative data of two samples (M14 and G14) is presented in Table 5. From Table 5, it is relevant to mention that there is a significant increase in the mass fraction of TiB_2 and hBN at and near the surface, after laser post-treatment (laser remelting of the surface). The occurrence of higher mass fraction of hBN and TiB_2 at and near the laser remelted surface, as compared to as-coated one, is attributed to their relatively lower specific gravity among the other constituents (cf. Table 6) and hence, their settlement at the near-surface region. This hypothesis is supported by the fact that the lower thermal conductivities of the coating materials (compared to that of the steel substrate) considerably extend the time for solidification of the melt pool, so that partial segregation of molten phases on the basis of density is a possibility. Similar observation was also reported earlier in literature [29].

4 Conclusions

1. Laser post-treatment tends to reduce defects in coating and make the top surface layer more compact by reducing pores.
2. There is a distinct increase in hardness at and near the top surface of the coating and hence the wear resistance increases due to laser post-treatment.

Table 6 Summary of the densities of the constituents in the coating

Name of the compound	Density (g/cm^3)
TiN	5.43
Al_2O_3	4.1
TiB_2	4.5
hBN	2.27

3. The coefficient of friction is reduced due to laser post-treatment.
4. Laser post-treatment reduces the detrimental effect of free hBN on the hardness and wear resistance of the coating while augmenting the favorable effect of free hBN on the friction coefficient.

Acknowledgments The authors would sincerely like to thank Mr. Sanjiv Maity of Department of Mechanical Engineering, IIT Kharagpur, West Bengal, India and the staff and members of the Central Research Facility (CRF), IIT Kharagpur, West Bengal, India for their involvement in the work. Authors would like to gratefully acknowledge the technical help obtained from Mr. Manish Tak of The International Advanced Research Centre for Powder Metallurgy and New Materials (ARCI), Hyderabad, India and Mr. Manoj Masanta of Department of Mechanical Engineering, IIT Kharagpur, West Bengal, India in carrying out the laser treatment of the samples and sample preparation. The authors would also like to thank Dr. Amod C. Umarikar, Head, School of Engineering, IIT Indore for his sincere support.

References

1. Mayrhofer PH, Mitterer C, Hultman L, Clemens H (2006) Microstructural design of hard coatings. Prog Mater Sci 51:1032–1114
2. Carrapichano JM, Gomes JR, Silva RF (2002) Tribological behaviour of Si_3N_4–BN ceramic materials for dry sliding applications. Wear 253:1070–1076
3. Yi G, Yan F (2006) Effect of hexagonal boron nitride and calcined petroleum coke on friction and wear behavior of phenolic resin-based friction composites. Mater Sci Eng A 425:330–338
4. Skopp A, Woydt M, Habig K-H (1995) Tribological behavior of silicon nitride materials under unlubricated sliding between 22°C and 1,000°C. Wear 181–183:571–580
5. Li JL, Xiong DS (2008) Tribological properties of nickel-based self-lubricating composite at elevated temperature and counterface material selection. Wear 265:533–539
6. Dutta Majumdar J, Manna I (2003) Laser processing of materials. Sadhana–Acad Proc Eng Sci 28:495–562
7. Pei YT, De Th M, Hosson J (2000) Functionally graded materials produced by laser cladding. Acta Mater 48:2617–2624
8. Subrahmanyam J, Vijayakumar M (1992) Self-propagating high-temperature synthesis. J Mater Sci 27:6249–6273
9. Borovinskaya IP (1992) Chemical classes of the SHS processes and materials. Pure Appl Chem 64:919–940
10. Merzhanov AG (1995) History and recent developments in SHS. Ceram Int 21:371–379
11. Morsi K (2001) Review: reaction synthesis processing of Ni-Al intermetallics. Mater Sci Eng A 299:1–15
12. Moore JJ, Feng HJ (1995) Combustion synthesis of advanced materials: Part I. Reaction parameters. Prog Mater Sci 39:243–273
13. Yang Y, Lan J, Li X (2004) Study on bulk aluminum matrix nano-composite fabricated by ultrasonic dispersion of nano-sized SiC particles in molten aluminum alloy. Mater Sci Eng A 380:378–383
14. Tjong SC, Ma ZY (2000) Microstructural and mechanical characteristics of in situ metal matrix composites. Mater Sci Eng R 29:49–113
15. Daniel BSS, Murthy VSR, Murty GS (1997) Metal-ceramic composites via in situ methods. J J Mater Process Technol 68:132–155
16. McCauley JW (1990) A historical and technical perspective on SHS. Ceram Eng Sci Proc 119:1137–1181
17. Shilyeav MI, Borzukh VE, Dorokhov AR (1994) On laser ignition of powder nickel aluminium systems. Fizika Goreniya I Vzryva 30:14–18
18. Slocombe A, Li L (2001) Selective laser sintering of TiC–Al_2O_3 composite with self-propagating high-temperature synthesis. J Mater Process Technol 118:173–178
19. Satyajit C, Shariff SM, Datta Majumdar J, Roy Choudhury A (2008) Development of nano-structured Al_2O_3-TiB_2-TiN coatings by combined SHS and laser surface alloying. Int J Adv Manuf Technol 38:938–943
20. Satyajit C, Ganesh P, Palai R, Wu JA, Kaul R, Dutta Majumdar J, Roy Choudhury A (2010) Effect of h-BN addition on the properties of nanostructured Al_2O_3–TiB_2–TiN based coatings developed by combined SHS and laser surface alloying. Surf CoatTechnol 204:1702–1709
21. Satyajit C, Shariff SM, Padmanabham G, Dutta Majumdar J, Roy Choudhury A (2010) Study on the effect of laser post-treatment on the properties of nanostructured Al_2O_3–TiB_2–TiN based coatings developed by combined SHS and laser surface alloying. Surf CoatTechnol 205:131–138
22. Satyajit C, Dutta Majumdar J, Singaiah K, Shariff SM, Padmanabham G, Roy Choudhury A (2011) Performance evaluation of laser surface alloyed hard nanostructured Al_2O_3–TiB_2–TiN composite coatings with in situ and ex situ reinforcements. Surf CoatTechnol 205:3478–3484
23. Zhang GJ, Ando M, Yang JF, Ohji T, Kanzaki S (2004) Boron carbide and nitride as reactants for in situ synthesis of boride-containing ceramic composites. J Eur Ceram Soc 24:171–178
24. Dutta Majumdar J, Manna I (2010) Mechanical properties of a laser-surface-alloyed magnesium-based alloy (AZ91) with nickel. Scr Mater 62:579–581
25. Mei QS, Lu K (2007) Melting and superheating of crystalline solids: from bulk to nanocrystals. Prog Mater Sci 52:1175–1262
26. Hou F, Wang W, Guo H (2006) Effect of the dispersibility of ZrO_2 nanoparticles in Ni–ZrO_2 electroplated nanocomposite coatings on the mechanical properties of nanocomposite coatings. Appl Surf Sci 252:3812–3817
27. Scattergood RO, Koch CC, Murty KL, Brenner D (2008) Strengthening mechanisms in nanocrystalline alloys. Mater Sci Eng A 493:3–11
28. Al-Jaroudi SS, Ul-Hamid A, Mohammed A-RI, Saner S (2007) Use of X-ray powder diffraction for quantitative analysis of carbonate rock reservoir samples. Powder Technol 175:115–121
29. Wong TT, Liang GY, He BL, Woo CH (2000) Wear resistance of laser-clad Ni–Cr–B–Si alloy on aluminium alloy. J Mater Process Technol 100:142–146